

Tikhonov regularization and prior information  
in electrical impedance tomography

M. Vauhkonen, D. Vadász, J.P. Kaipio,  
E. Somersalo and P.A. Karjalainen

April 9, 1996

Report No. 3/96

Submitted to *IEEE Trans. Medical Imaging*

University of Kuopio • Department of Applied Physics  
P.O.Box 1627, FIN-70211 Kuopio, Finland

# Tikhonov regularization and prior information in electrical impedance tomography

M. Vauhkonen\*, D. Vadász†, J.P. Kaipio, E. Somersalo‡ and P.A. Karjalainen

April 9, 1996

**Abstract** The solution of impedance distribution in electrical impedance tomography is a nonlinear inverse problem that requires the use of a regularization method. The generalized Tikhonov regularization methods have been popular in the solution of many inverse problems. The regularization matrices that are usually used with the Tikhonov method are more or less ad hoc and the implicit prior assumptions are thus in many cases inappropriate. In this paper we propose an approach to the construction of the regularization matrix that conforms to the prior assumptions on the impedance distribution. The approach is based on the construction of an approximating subspace for the expected impedance distributions. It is shown by simulations that the reconstructions obtained with the proposed method are better than with two other schemes of the same type when the prior is correct. On the other hand, when the prior is completely incorrect, the method will still yield results that are only slightly worse than with ad hoc priors.

## 1 Introduction

In electrical impedance tomography (EIT) different current patterns are applied to the body through electrodes that are attached on the surface and the corresponding voltages are measured. Based on this boundary data the internal impedance (resistivity, conductivity) distribution or changes in it can be approximated [1, 2].

EIT image reconstruction is a nonlinear ill-posed inverse problem for which reason we have to use regularization techniques to obtain stable solutions. The so-called Tikhonov-regularized versions of the EIT inverse problem can be written in the form

$$\min_{\rho} \left\{ \|V - U(\rho)\|^2 + \alpha \|L\rho\|^2 \right\}, \quad (1)$$

where  $\rho$  is the resistivity distribution,  $U(\rho)$  is the resistivity to potential mapping, that is, the potentials obtained from the model with known  $\rho$ ,  $V$  are the measured potentials,  $L$  is a so-called regularization matrix and  $\alpha$  is a regularization parameter. For the EIT electrode model and the corresponding finite element approximation that are used in this paper, see Appendix A.

The most often used regularization matrices in EIT are the identity matrix and the matrices corresponding to the first and second difference operators [3, 4, 5]. The implicit prior assumptions when these matrices are used are that  $\rho$  is either small, slowly changing or smooth, respectively. A different type of prior has been used in [6] in which the unknown conductivity is assumed to be “blocky”. The blockiness refers to that the conductivity is a piecewise constant function, and thus has sharp edges. The corresponding reconstruction method is based on selecting a conductivity distribution that has the least total variation from all conductivities that are consistent with the measured data. These can be taken as representations of prior information and in some cases these priors are inappropriate.

---

\*M. Vauhkonen, J.P. Kaipio and P.A. Karjalainen are with the Department of Applied Physics, University of Kuopio, P.O.Box 1627, FIN-70211 Kuopio, Finland. M. Vauhkonen is also with the Department of Mathematical Sciences, University of Oulu, Linnanmaa, P.O. Box 333, FIN-90571 Oulu, Finland

†D. Vadász is with the Department of Electromagnetic Theory, Technical University of Budapest, Egry József út 18, H-1521 Budapest, Hungary

‡E. Somersalo is with the Department of Mathematics, Helsinki University of Technology, Otakaari 1, FIN-02150, Finland

It is also possible to include other kind of prior information into image reconstruction. Prior information in EIT can be anatomical data obtained e.g. from MRI together with known resistivities of different tissues and also the noise level of the measurement system. These priors have been used successfully in [7, 8, 9, 10, 11, 12].

In [11, 12] it was assumed that the resistivity distribution could be well approximated as a linear combination of some preselected basis functions  $w_m$ , that is,  $\rho = \sum_{m=1}^M c_m w_m(x)$ ,  $c_m \in \mathbb{R}$ , where  $M$  is small, e.g. 3-5. Prior information on the structures and conductivities were used for the construction of these basis functions. The disadvantage of this method is that one obtains misleading results when prior information is not correct. With misleading we mean that one obtains those structures that are in  $w_m$  in reconstructed image, even if they do not actually exist.

In this paper we use the same kind of idea but we do not force the solution to be in the subspace  $S_w$  spanned by the basis functions  $w_m$ , as in [11, 12], but instead we only “draw” the solution towards it. This can be done using the generalized Tikhonov regularization method with properly constructed regularization matrix  $L$ . With this improvement we can partially avoid misleading results even if the prior information is not correct.

In this study we have compared this method with two other regularization methods. The first one is the method introduced in [5], which is near to the standard Tikhonov regularization method (called STRM in this paper), where  $L = I$  (identity matrix). The second is the method where the norm  $\|L\rho\|$  approximates the total variation of the distribution  $\rho$  [6]. In the sequel this method is called the minimum total variation method (MTVM).

## 2 Construction of the regularization matrices

One way in which the generalized Tikhonov regularization method can be understood to work, is that it draws the solution towards the null space  $\mathcal{N}(L)$  of the regularization matrix  $L$  (more detailed analysis is presented in section 3) [13, 14]. If we use, for example, the first or the second difference matrices, we draw the solution towards a uniform distribution or towards the combination of a uniform and a planar distribution, respectively. This is because these form the basis for the null spaces of these matrices.

If we have information on the true resistivity distribution, the regularization matrix can be constructed in such a way that the solution is drawn towards the known distribution by the regularization. The procedure how this is done is presented in the following sections.

### 2.1 Subspace regularization method

Let us consider first a procedure for the construction of the subspace  $S_w$ , in which (or near which) the true solution is assumed to lie, more detailed description can be found in [11]. First we form a set of expectable resistivity distributions (vectors)  $\rho_n$ ,  $n = 1, \dots, N$ , near which the true resistivity distribution is assumed to be. For this we can use the data obtained e.g. from MRI and from earlier measured resistivity values [12, 15]. This set of distributions is called the learning set. For this learning set we calculate the covariance matrix  $\Gamma$

$$\Gamma = N^{-1} \hat{\rho} \hat{\rho}^T,$$

where the matrix  $\hat{\rho} = [\rho_1, \dots, \rho_N] \in \mathbb{R}^{P \times N}$ , where  $P$  refers to the number of discretized elements in the finite element mesh. To find the  $M \ll N$  dimensional subspace in which the learning set can be approximated with the smallest mean square error, we calculate the  $M$  largest eigenvalues and the corresponding orthonormal eigenvectors  $w_m$ ,  $m = 1, \dots, M$  of  $\Gamma$ . This can be done using the orthogonal iteration method [16]. This method can be implemented in such a way that one does not have to evaluate  $\Gamma$  at all, not to speak of the calculation of the all eigenvectors and eigenvalues of it. These  $M$  eigenvectors span the subspace  $S_w$ . This kind of a procedure is widely known as Principal Component Analysis (PCA) [17].

We could force the solution to be in  $S_w$ , that is,  $\rho = \sum_{m=1}^M c_m w_m$ ,  $c_m \in \mathbb{R}$ , as was done in [11, 12]. However, if our prior assumptions about the resistivity distribution are not correct, we obtain misleading results. This can be avoided using regularization of the form (1).

In the subspace regularization method (SSRM) we minimize the functional (1) with respect to  $\rho$  and use the regularization matrix  $L$  whose null space is  $S_w$ . The matrix of this form can be shown to be

$$L = I - WW^T, \quad (2)$$

where  $I$  is the identity matrix and  $W$  is the matrix having the vectors  $w_m$ ,  $m = 1, \dots, M$  as its columns. Using a matrix  $L$  of this form the solution can be drawn towards  $S_w$  as will be explained in more detail in Section 3.

For the solution of (1) we have used a Newton's type method and after the linearization we have the iteration

$$\rho_{i+1} = \rho_i + \Delta\rho_i, \quad (3)$$

where

$$\begin{aligned} \Delta\rho_i &= -H^{-1}\nabla\Phi \\ &= (J^T J + \alpha L^T L)^{-1} [J^T (V - U(\rho_i)) - \alpha L^T L \rho_i], \end{aligned} \quad (4)$$

where  $H$  is the modified Hessian matrix of  $\Phi(\rho_i)$ ,  $\nabla\Phi$  is the gradient of  $\Phi(\rho_i)$ ,  $J$  is the Jacobian of the mapping  $U(\rho)$  and  $(\cdot)^T$  denotes transpose. In (4) we have left out the second derivatives with respect to  $\rho$  of the mapping  $U(\rho)$ . In simulations we have used only one step of the iteration (3).

## 2.2 Other regularization methods

For the comparison of the SSRM with methods proposed earlier, we have used two other regularization approaches. In the first one the regularization matrix is a simple diagonal weighting for  $J^T J$  and the equation for the increment  $\Delta\rho_i$  is, [5, 18]

$$\Delta\rho_i = (J^T J + \alpha \text{diag}(J^T J))^{-1} [J^T (V_0 - U(\rho_i))] ,$$

where  $\text{diag}(\cdot)$  denotes the diagonal matrix and can here also be thought to represent an approximation for the missing part of the second derivative of the mapping  $U(\rho)$ .

In MTVM the regularization matrix has to correspond to the discretization of the domain to be analysed and it is obtained as follows. Let the length of each edge  $i$  between adjacent pixels be  $d_i$ ,  $i = 1, \dots, I$  (Fig. 1 b). The  $i$ 'th row of the matrix  $L \in \mathbb{R}^{I \times P}$  is chosen to be

$$L_i = [0, \dots, 0, 1, \dots, 0, -1, 0, \dots, 0] ,$$

where 1 and  $-1$  are placed in the columns corresponding to the pixels with the common edge  $i$ , see Fig. 1 b). The term  $\|L\rho\|$  gives an approximation for the total variation of the distribution  $\rho$ , [6]. In addition, each row of  $L_i$  has been weighted with the length  $d_i$  of the edge  $i$ . The final form of increment  $\Delta\rho_i$  is then

$$\begin{aligned} \Delta\rho_i &= (J^T J + \alpha L^T D^T D L)^{-1} \\ &\quad [J^T (V_0 - U(\rho_i)) - \alpha L^T D^T D L \rho_i] , \end{aligned}$$

where  $D$  is the diagonal matrix with the vector  $d$  as the diagonal.

## 3 Analysis of the SSRM

Let us consider the first step of iteration (4), that is,  $i = 0$ . If the initial value  $\rho_0$  is in the null space of the matrix  $L$ , that is,  $L\rho_0 = 0$  we obtain

$$\rho_1 - \rho_0 = (J^T J + \alpha L^T L)^{-1} [J^T (V - U(\rho_0))] ,$$

which is the solution to the linearized problem

$$\min_{\delta\rho} \left\{ \|\delta V - J\delta\rho\|^2 + \alpha \|L\delta\rho\|^2 \right\} , \quad (5)$$

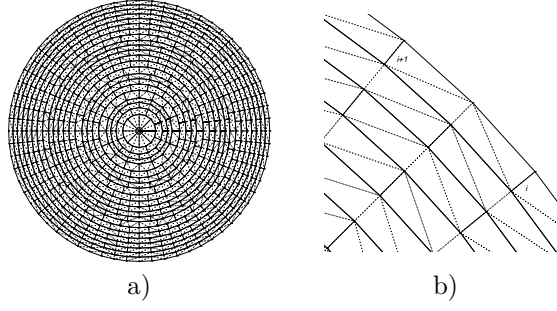


**Figure 1:** In a) there is the grid used in the forward (triangles with solid/dotted lines) and the inverse problem (quadrilaterals with solid lines). In b) there is the  $i$ 'th and  $i + 1$ 'th edge between adjacent elements. Used in the MTVM.

where  $\delta V = V - U(\rho_0)$  is a vector of differences between measured voltages  $V$  and calculated voltages  $U(\rho_0)$ . A difference in resistivity is  $\delta\rho = \rho_1 - \rho_0$ .

The reason why the regularization method draws the solution towards the null space of  $L$  can be understood by considering the generalized singular values (GSVD) of the matrix pair  $(J, L)$ ,  $J \in \mathbb{R}^{m \times n}$ ,  $L \in \mathbb{R}^{p \times n}$  and  $r = \text{rank}(L)$  [13, 14]

$$\begin{pmatrix} J \\ L \end{pmatrix} = \begin{pmatrix} \mathcal{U} & 0 \\ 0 & \mathcal{V} \end{pmatrix} \begin{pmatrix} \text{diag}(\gamma_i) & 0 \\ 0 & I_{n-r} \\ \text{diag}(\tau_i) & 0 \end{pmatrix} \mathcal{X}^{-1},$$

where the matrices  $\mathcal{U}, \mathcal{V}, \mathcal{X}$  are given by

$$\begin{aligned} \mathcal{U} &= (\mathbf{u}_1, \dots, \mathbf{u}_n) \in \mathbb{R}^{m \times n} \\ \mathcal{V} &= (\mathbf{v}_1, \dots, \mathbf{v}_p) \in \mathbb{R}^{p \times p} \\ \mathcal{X} &= (\mathbf{x}_1, \dots, \mathbf{x}_n) \in \mathbb{R}^{n \times n} \end{aligned}$$

and the vectors  $\mathbf{u}_i, \mathbf{v}_i$  are orthonormal and  $\mathbf{x}_i$  are linearly independent. Moreover,  $\text{diag}(\gamma_i)$  and  $\text{diag}(\tau_i)$  denote  $r \times r$  diagonal matrices with positive diagonal entries. The generalized singular values of the pair  $(J, L)$  are then defined as the ratios  $\eta_i = \gamma_i / \tau_i$ , which are assumed to be in non-increasing order, that is

$$\eta_1 \geq \eta_2 \geq \dots \geq \eta_r > 0$$

Now we can write down the formula for the regularized solution to (5)

$$\delta\rho = \sum_{i=1}^r \psi(\eta_i^2) \frac{\mathbf{u}_i^T \delta V}{\gamma_i} \mathbf{x}_i + \sum_{i=r+1}^n \mathbf{u}_i^T \delta V \mathbf{x}_i, \quad (6)$$

where

$$\psi(\lambda) = \frac{\lambda}{\lambda + \alpha}$$

is the Tikhonov filter function [14]. We observe that the formula (6) contains two components. The second, that is given by

$$\delta\rho_2 = \sum_{i=r+1}^n \mathbf{u}_i^T \delta V \mathbf{x}_i$$

is the component of the solution in the null space of  $L$  and is not, in a straightforward manner, affected by the regularization. The first component depends on the regularization parameter  $\alpha$  via the filter function  $\psi$ . Considering these facts we can understand the idea behind the SSRM. As we increase the regularization parameter, we decrease the effect of the first term and increase the overall effect of the second term, which is the part of the solution in the null space of  $L$ .

Two extreme situations of (6) are those in which  $\alpha \rightarrow 0$  and  $\alpha \rightarrow \infty$ . The first case is the ordinary (linearized) LS (Least Squares) problem, for which the solution is

$$\delta\rho = \sum_{i=1}^n \frac{\mathbf{u}_i^T \delta V}{\gamma_i} \mathbf{x}_i$$

and the second one, when  $\alpha \rightarrow \infty$ , is the LS problem with equality constraint

$$\min_{\delta\rho} \|\delta V - J\delta\rho\|^2 \quad \text{so that} \quad L\delta\rho = 0$$

the solution of which is

$$\delta\rho = \sum_{i=r+1}^n \mathbf{u}_i^T \delta V \mathbf{x}_i .$$

This is just the part of the solution which is in the null space of  $L$  and is the same as the range of  $W$ , that is, the solution is in the subspace spanned by the vectors  $w_1, \dots, w_m$  [12].

*Remark 1.* One way to implement prior information into the Tikhonov regularization can be obtained by replacing  $\|L\rho\|$  in (1) with  $\|\rho - \rho^*\|$  where  $\rho^*$  is the assumed distribution. This is a special case of a more general regularization approach presented in this Section.

*Remark 2.* Statistically the solution to (1) corresponds to the *Maximum A Posteriori* (MAP) estimate for random parameters  $\rho$  [19]. The prior assumption about  $\rho$  is then that it is a Gaussian random variable with  $\rho \sim N(0, \alpha^{-1}(L^T L)^{-1})$ . Hence in SSRM the prior assumption in statistical sense is formally  $\rho \sim N(0, \alpha^{-1}(I - WW^T)^{-1})$ . However, the matrix  $(I - WW^T)$  is singular and the variance of  $\rho$  is thus infinite in certain directions. This means that the prior distribution for the estimate is (partially) uninformative [19].

#### 4 Solving the forward problem and the Jacobian $J$

In the iteration (3) we have to solve the forward problem, that is, the potentials  $U(\rho_i)$  and the Jacobian of the mapping  $U(\rho)$ . In this study the forward problem has been calculated by the complete electrode model [20, 21, 22], see Appendix A. Since analytical solution for this model can not be obtained, we have used the finite element method (FEM) [22, 8, 23].

In FEM we form a linear system

$$Ab = f , \tag{7}$$

where  $A \in \mathbb{R}^{(N+L-1) \times (N+L-1)}$  is the master matrix including integrations over the elements and over the boundary of the object,  $b \in \mathbb{R}^{N+L-1 \times 1}$  is the vector in which the  $N$  first elements are the voltages in each node and the last  $L-1$  the voltages on the electrodes and  $f \in \mathbb{R}^{N+L-1 \times 1}$  is the vector in which the first  $N$  are zeros (no internal current generators) and the last  $L-1$  elements contain the injected currents. After solving  $b$  from (7) we can extract the voltages

In this study we have used a mesh of 1984 triangular elements,  $N = 1025$  nodes and  $L = 32$  electrodes for the forward calculations and 496 elements for the inverse solution, Fig. 1. The triangular elements have been grouped in order to have the same area for each element in the inverse solution, as was done in [5, 18]. For more details about the FEM used in this study, see Appendix A. For the current injection we have used trigonometric current patterns, that is,

$$I_l^k = \begin{cases} \cos(k\zeta_l) & l = 1, \dots, 32, k = 1, \dots, 16 \\ \sin((k-16)\zeta_l) & l = 1, \dots, 32, k = 17, \dots, 31 \end{cases} , \tag{8}$$

where  $\zeta_l = 2\pi l/32$ .

In (4) we need the derivatives of the mapping  $U(\rho)$  with respect to  $\rho$ , that is, the Jacobian  $J$ . We have used the so-called standard method to obtain the derivatives [24]. Since we used 31 different current patterns with 32 electrodes and the number of estimated parameters is 496, the size of  $J$  is  $992 \times 496$ . The  $j$ 'th column of  $J$ , that is, the derivatives  $\partial U / \partial \rho_j$  can be obtained from [24]

$$\frac{\partial U}{\partial \rho_j} = -A^{-1} \frac{\partial A}{\partial \rho_j} U , \tag{9}$$

where  $U$  is the matrix with the calculated voltages that correspond to each current pattern as its columns. From (9) we need to extract the part that belongs to the electrodes, namely 31 last rows. Using the formula (14) in Appendix A, we obtain the derivatives with respect to each electrode. Therefore we have obtained a  $32 \times 31$  matrix which is expanded to a vector form and is the first column of  $J$ . The term  $\partial A / \partial \rho_j$  in (9) is straightforward to calculate.

## 5 Results

We constructed two test distributions and simulated the measured voltages using the complete electrode model and the trigonometric current patterns. The first simulated distribution was a thorax model in which case we used correct prior, Fig. 3, and the second one was a distribution in which the prior was incorrect, Fig. 4. To the simulated voltages we added some uniformly distributed random noise. The noise levels were  $\pm 1\%$  or  $\pm 3\%$  of the corresponding measured voltage. These noise levels were chosen to correspond to the typical noise levels in measurement systems, (1% of the smallest potential measured, [9]).

The inverse problem was solved using the regularization procedures described in previous sections. We used only one step of the iteration and the first guess  $\rho_0$  was uniform, corresponding to the background resistivity value.

In both simulations we used the same regularization matrix in SSRM. The prior that we used in the calculation of  $\Gamma$  included the (simulated) heart and the lungs in different states, modified from the distribution shown in the Fig. 3. The number of different resistivity vectors in the learning set was 81. In the matrix  $W$  in (2) we used three ( $M = 3$ ) largest eigenvectors of the matrix  $\Gamma$ . This was chosen since in [12] it was found that we should not exceed  $M = 3$  when noise level is 3% of measured voltages. These eigenvectors are shown in Fig. 2.

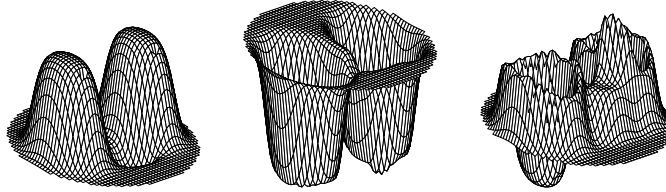


**Figure 2:** The eigenvectors corresponding to the three largest eigenvalues of the covariance  $\Gamma$ . The “heart” is on the front of the image.

The results from the simulated thorax resistivity distribution are shown in Fig. 3. The distribution was taken from the learning set and the ratios of the resistivities of the spine, lungs, muscle/fat and heart were  $3.75 : 1.75 : 1 : 0.75$ , respectively. The background resistivity  $\rho_0$  was the resistivity of the muscle/fat.

As can be seen, the best result is obtained with the SSRM. The ability of SSRM to handle noise, when the prior is correct, can also be seen in Fig. 3. The noise added to the measured voltages has only a small effect on the reconstruction made by SSRM and on the other hand, the two other methods are quite blurred because of large amount of regularization. The parameters  $\alpha$  were adjusted experimentally for each case and they were between 0.06–0.2 in SSRM, 0.6–1.8 in STRM and 0.4–2.4 in MTVM, depending on the level of the noise. If we compare STRM with MTVM, we see that a very simple diagonal weighting, proposed in [5], gives as good results as more complicated MTVM method.

The results from another simulated distribution, in which the prior used in SSRM is incorrect, are shown in Fig. 4. The resistivity ratios of the upper piece of perturbation, background and the lower piece of perturbation were  $1.5 : 1 : 0.7$ . The background resistivity  $\rho_0$  was the unity distribution.

In this the SSRM was modified to leave out, the term  $L\rho_0$  in 4 since the true distribution was so far from the prior and the uniform distribution  $\rho_0$  was not in the null space of  $L$ . We could have done this also in the previous example without having any negative effects.

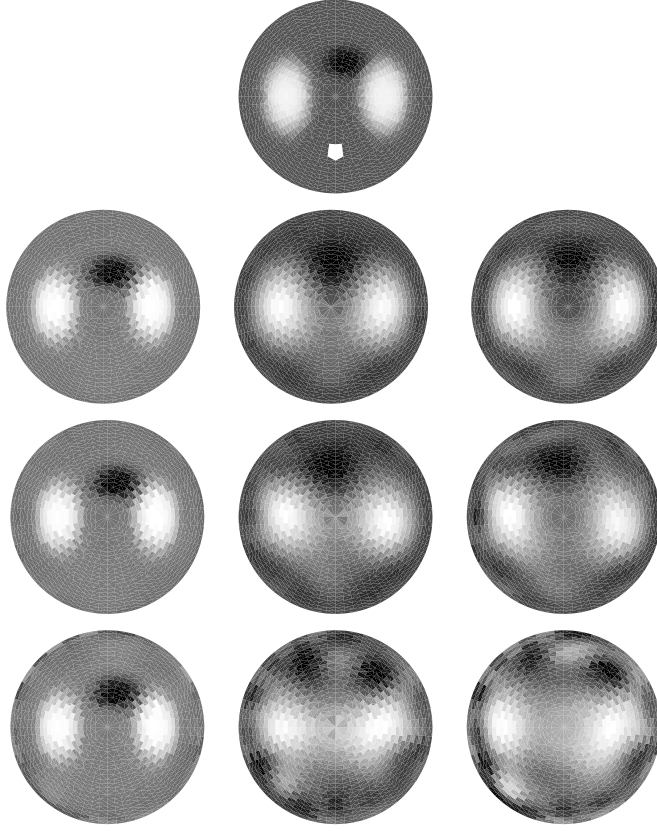


**Figure 3:** On the top: The simulated distribution taken from learning set  $\hat{p}$ . In the first row, the solutions without noise using the SSRM, STRM and MTVM, respectively. In the next row, the same, but with  $\pm 1\%$  noise added and in the last row with  $\pm 3\%$  noise added.

From Fig. 4 (first column) we see what happens when our prior is incorrect. When we increase the amount of regularization due to the noise, in order to stabilize the solution, at the same time we increase the visibility of the structures which were in the learning set. For this reason we can not use as large regularization parameters in SSRM as in the situation in Fig. 3. The regularization parameters were 0.003–0.015 in SSRM, 0.4–3 in STRM and 0.3–3.5 in MTVM.

There are several methods for choosing in some sense optimal regularization parameter  $\alpha$  [14]. These are for example the *discrepancy principle* and the *Grefere/Raus-method* when the level of measurement noise is known and the *quasi-optimality criterion*, the *generalized cross validation* and the *L-curve criterion* when the noise level is unknown. The different criteria will, however, yield results of different optimality. Since we knew the true distribution in the simulations, we selected the regularization parameter in such a way that we obtain the best result. When the true distribution is unknown, an implementation of these methods is recommended.

## 6 Discussion

A novel method for using prior information in the regularized electrical impedance tomography reconstruction algorithm has been proposed and compared to two other regularization methods. When the prior is correct we see from the simulation that SSRM gives more realistic qualitative estimate e.g. in the heart area than the two other methods. The ability of the SSRM to handle noise can be seen from the simulations when 1% or 3% of noise is added to the simulated voltages. When the prior is correct, noise has only a small effect on the reconstruction but when we are far from the prior, we increase the visibility of unwanted structures which were in the learning set, as



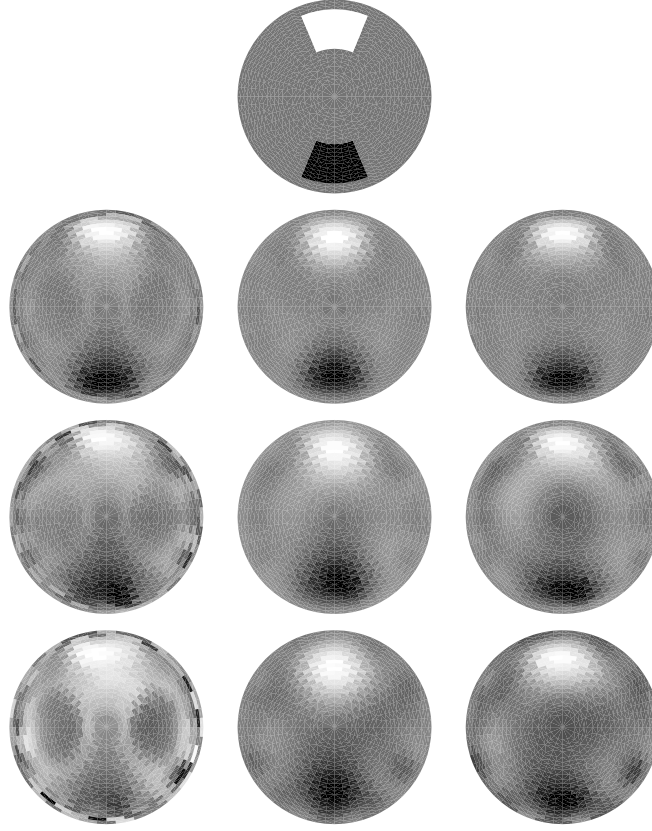


**Figure 4:** On the top: The true resistivity distribution. In the first row the solutions without noise using the SSRM, STRM and MTVM, respectively. In the next row, the same, but with  $\pm 1\%$  noise added and in the last row with  $\pm 3\%$  noise added.

we increase the regularization parameter. There is a possibility to check if it is reasonable to use SSRM at all by projecting the result to the  $S_w$  and checking if that part of the solution is large enough. If not, that is, we are far from the subspace, we should use some other regularization matrix or teach the system again with this new feature. Using this learning we could obtain iterative version of the proposed method.

## Appendix A

Let the  $\Omega$  be a two dimensional object to imaged and  $\partial\Omega$  the boundary of  $\Omega$ . The complete electrode model consists of the equations

$$\begin{aligned} \nabla \cdot (\sigma \nabla u) &= 0 & \text{in } \Omega \\ u + z_l \sigma \frac{\partial u}{\partial \nu} &= U_l & \text{on } e_l, l = 1, 2, \dots, L \\ \int_{e_l} \sigma \frac{\partial u}{\partial \nu} dS &= I_l & l = 1, 2, \dots, L \\ \sigma \frac{\partial u}{\partial \nu} &= 0 & \text{on } \partial\Omega \setminus \cup_{l=1}^L e_l \end{aligned}$$

where  $u = u(x)$ ,  $x = (x_1, x_2)$  is electric potential,  $\sigma = \sigma(x)$  is conductivity (assumed to be real),  $e_l$  is  $l$ 'th electrode,  $z_l$  is effective contact impedance between  $l$ 'th electrode and tissue (also real),  $U_l$  are the voltages on the electrodes,  $I_l$  are the injected currents and  $\nu$  is outward unit normal. In

addition we need the following two conditions for the injected current and measured voltages

$$\begin{aligned}\sum_{l=1}^L I_l &= 0 \\ \sum_{l=1}^L U_l &= 0\end{aligned}$$

For  $u(x)$  we write the finite element approximation  $u^h$  in the form

$$u^h = \sum_{i=1}^N \alpha_i \varphi_i, \quad (10)$$

where  $\varphi_i = \varphi_i(x)$  are piecewise linear basis functions. For the voltages  $U$  on the electrodes we use the approximation

$$U^h = \sum_{j=1}^{L-1} \beta_j n_j \quad (11)$$

where  $n_1 = [1, -1, 0, \dots, 0]^T$ ,  $n_2 = [1, 0, -1, 0, \dots, 0]^T \in \mathbb{R}^{L \times 1}$ , etc. This means that the first electrode is the reference. Note that every vector  $n_j$  whose sum vanishes can be used. In (10)  $N$  is a number of nodes in the finite element mesh and  $\alpha_i$  are the coefficients to be determined and in (11)  $L$  is a number of electrodes and  $\beta_j$  are the coefficients to be determined.

In [21] Somersalo *et al.* have shown that for any  $(v, V)$

$$B_s((u, U), (v, V)) = \sum_{l=1}^L I_l V_l,$$

where  $B_s$  is the sesquilinear form defined as

$$B_s = \int_{\Omega} \sigma \nabla u \cdot \nabla v \, dx + \sum_{l=1}^L \frac{1}{z_l} \int_{e_l} (u - U_l)(v - V_l) \, dS, \quad (12)$$

for details we refer to [21].

Now, using the theory of finite element methods [25], we construct a matrix equation

$$Ab = f \quad (13)$$

such that  $b = (\alpha_i, \beta_j)^T$  is  $(N + L - 1) \times 1$  vector and  $A$  is the master matrix

$$A = \begin{pmatrix} & & & \vdots & & \\ & B & & \vdots & C & \\ & & & \vdots & & \\ \cdots & \cdots & \cdots & \cdots & \cdots & \cdots \\ & & & \vdots & & \\ & C^T & & \vdots & D & \\ & & & \vdots & & \end{pmatrix}$$

When we substitute the FEM basis functions  $\varphi_i$  to the sesquilinear form (12), we obtain the matrix elements

$$B(i, j) = \int_{\Omega} \sigma \nabla \varphi_i \cdot \nabla \varphi_j \, dx + \sum_{l=1}^L \frac{1}{z_l} \int_{e_l} \varphi_i \varphi_j \, dS,$$

$$\begin{aligned}
i, j &= 1, 2, \dots, N \\
C(i, j) &= - \left( \frac{1}{z_1} \int_{e_1} \varphi_i dS - \frac{1}{z_{j+1}} \int_{e_{j+1}} \varphi_{i+1} dS \right), \\
i &= 1, 2, \dots, N, \quad j = 1, 2, \dots, L-1 \\
D(i, j) &= \sum_{l=1}^L \frac{1}{z_l} \int_{e_l} (n_i)_l (n_j)_l dS \\
&= \begin{cases} \frac{|e_i|}{z_1}, & m \neq j \\ \frac{|e_i|}{z_1} + \frac{|e_{j+1}|}{z_{j+1}}, & m = j \end{cases}, \quad i, j = 1, 2, \dots, L-1
\end{aligned}$$

The data vector on the right hand side of (13) is

$$f = \left[ \mathbf{0}, \sum_{l=1}^L I_l (n_j)_l \right] = [\mathbf{0}, I]^T,$$

where  $\mathbf{0} = [0, \dots, 0] \in \mathbb{R}^{1 \times N}$  and  $I = [I_1 - I_2, I_1 - I_3, \dots, I_1 - I_L] \in \mathbb{R}^{1 \times (L-1)}$  contains the injected currents.

After solving vector  $b$  and whence  $\beta_j$  we use equation (11) to find the potentials  $U_l^h$  on the electrodes. They can be calculated as

$$\begin{aligned}
U_1^h &= \sum_{l=1}^{L-1} \beta_l \\
U_2^h &= -\beta_1 \\
U_3^h &= -\beta_2 \\
&\vdots \\
U_L^h &= -\beta_{L-1}
\end{aligned} \tag{14}$$

## References

- [1] A.P. Calderon, "On an inverse boundary value problem", in *Seminar on Numerical Analysis and its Applications to Continuum Physics*, W.H. Meyer and M.A. Raupp, Eds., Rio de Janeiro, 1980, pp. 65–73, Brazilian Math. Society.
- [2] D.C. Barber and B.H. Brown, "Applied potential tomography", *J Phys E: Sci Instrum*, vol. 17, pp. 723–733, 1984.
- [3] P. Hua, E.J. Woo, J.G. Webster, and W.J. Tompkins, "Iterative reconstruction methods using regularization and optimal current patterns in electrical impedance tomography", *IEEE Trans Med Imaging*, vol. 10, pp. 621–628, 1991.
- [4] P. Hua, J.G. Webster, and W.J. Tompkins, "A regularised electrical impedance tomography reconstruction algorithm", *Clin Phys Physiol Meas, Suppl A*, vol. 9, pp. 137–141, 1988.
- [5] M. Cheney, D. Isaacson, J.C. Newell, S. Simske, and J. Goble, "NOSER: An algorithm for solving the inverse conductivity problem", *Internat. J. Imaging Systems and Technology*, vol. 2, pp. 66–75, 1990.
- [6] D.C. Dobson and F. Santosa, "An image enhancement technique for electrical impedance tomography", Tech. Rep., Institute for mathematics and its applications, University of Minnesota, 1993.
- [7] E.J. Woo, P. Hua, J.G. Webster, and W.J. Tompkins, "Measuring lung resistivity using electrical impedance tomography", *IEEE Trans Biomed Eng*, vol. 39, pp. 756–760, 1992.
- [8] E.J. Woo, P. Hua, J.G. Webster, and W.J. Tompkins, "Finite-element method in electrical impedance tomography", *Med Biol Eng Comput*, vol. 32, pp. 530–536, 1994.
- [9] B.M. Eyüboğlu, T.C. Pilkington, and P.D. Wolf, "Estimation of tissue resistivities from multiple-electrode impedance measurements", *Phys Med Biol*, vol. 39, pp. 1–17, 1994.
- [10] M. Glidewell and K.T. Ng, "Anatomically constrained electrical impedance tomography for anisotropic bodies via a two-step approach", *IEEE Trans Med Imaging*, vol. 14, pp. 498–503, 1995.
- [11] M. Vauhkonen, J.P. Kaipio, E. Somersalo, and P.A. Karjalainen, "Electrical impedance tomography with basis constraints", Tech. Rep. 2/95, University of Kuopio, Department of Applied Physics, 1995.

- [12] M. Vauhkonen, J.P. Kaipio, E. Somersalo, and P. A. Karjalainen, "Basis constraint method for estimating conductivity distribution of the human thorax", in *Proceedings of the IX International Conference on Electrical Bio-Impedance*, 1995, pp. 528–531.
- [13] C.F. van Loan, "Generalizing the singular value decomposition", *SIAM J Numer Anal*, vol. 13, pp. 76–83, 1976.
- [14] M. Hanke and P.C. Hansen, "Regularization methods for large-scale problems", *Surv Math Ind*, vol. 3, pp. 253–315, 1993.
- [15] L.A. Geddes and L.E. Baker, "The specific resistance of biological material– a compendium of data for the biomedical engineering and physiologist", *Med Biol Eng*, vol. 5, pp. 271–293, 1967.
- [16] G.H. Golub and C.H. van Loan, *Matrix Computations*, The Johns Hopkins University Press, 1989.
- [17] I.T. Jolliffe, *Principal Component Analysis*, Springer-Verlag, 1986.
- [18] P.M. Edic, *The implementation of a real-time electrical impedance tomograph*, PhD thesis, Rensselaer Polytechnic Institute, Troy, New York, 1994.
- [19] A. Tarantola, *Inverse Problem Theory*, Elsevier, 1987.
- [20] K.-S. Cheng, D. Isaacson, J.C. Newell, and D.G. Gisser, "Electrode models for electric current computed tomography", *IEEE Trans Biomed Eng*, vol. 36, pp. 918–924, 1989.
- [21] E. Somersalo, M. Cheney, and D. Isaacson, "Existence and uniqueness for electrode models for electric current computed tomography", *SIAM J Appl Math*, vol. 52, pp. 1023–1040, 1992.
- [22] K. Paulson, W. Breckon, and M. Pidcock, "Electrode modelling in electrical impedance tomography", *SIAM J Appl Math*, vol. 52, pp. 1012–1022, 1992.
- [23] P. Hua, E.J. Woo, J.G. Webster, and W.J. Tompkins, "Finite element modeling of electrode–skin contact impedance in electrical impedance tomography", *IEEE Trans Biomed Eng*, vol. 40, pp. 335–343, 1993.
- [24] T.J. Yorkey, J.G. Webster, and W.J. Tompkins, "Comparing reconstruction algorithms for electrical impedance tomography", *IEEE Trans Biomed Eng*, vol. 34, pp. 843–852, 1987.
- [25] S.C. Brenner and L.R. Scott, *The Mathematical Theory of Finite Element Methods*, Springer, 1994.